Petroleum Science 19 (2022) 1460–1472

Contents lists available at ScienceDirect

Petroleum Science

journal homepage: www.keaipublishing.com/en/journals/petroleum-science

Original Paper

Organic matter occurrence and pore-forming mechanisms in lacustrine shales in China

Li-Chun Kuang [a, *], Lian-Hua Hou [b, c, **], Song-Tao Wu [b, c, d], Jing-Wei Cui [b, c, d], Hua Tian [b, c, d], Li-Jun Zhang [b], Zhong-Ying Zhao [b], Xia Luo [b], Xiao-Hua Jiang [b, c, d]

[a] Science and Technology R&D Department, CNPC, Beijing, 100000, China
[b] Research Institute of Petroleum Exploration and Development, CNPC, Beijing, 100083, China
[c] National Energy Tight Oil and Gas R&D Center, Beijing, 100083, China
[d] Key Laboratory of Oil and Gas Reservoirs, CNPC, Beijing, 100083, China

ARTICLE INFO

Article history:
Received 10 May 2021
Accepted 15 November 2021
Available online 8 March 2022

Edited by Jie Hao and Teng Zhu

Keywords:
Shale oil
Unconventional oil and gas
Organic matter
Pore evolution
Log interpretation model

ABSTRACT

The evolution of pore structure in shales is affected by both the thermal evolution of organic matter (OM) and by inorganic diagenesis, resulting in a wide variety of pore structures. This paper examines the OM distribution in lacustrine shales and its influence on pore structure, and describes the process of porosity development. The principal findings are: (i) Three distribution patterns of OM in lacustrine shales are distinguished; laminated continuous distribution, clumped distribution, and stellate scattered distribution. The differences in total organic carbon (TOC) content, free hydrocarbon content (S_1), and OM porosity among these distribution patterns are discussed. (ii) Porosity is negatively correlated with TOC and plagioclase content and positively correlated with quartz, dolomite, and clay mineral content. (iii) Pore evolution in lacustrine shales is characterized by a sequence of decreasing-increasing-decreasing porosity, followed by continuously increasing porosity until a relatively stable condition is reached. (iv) A new model for evaluating porosity in lacustrine shales is proposed. Using this model, the organic and inorganic porosity of shales in the Permian Lucaogou Formation are calculated to be 2.5%–5% and 1%–6.3%, respectively, which correlate closely with measured data. These findings may provide a scientific basis and technical support for the sweet spotting in lacustrine shales in China.

1. Introduction

Lacustrine shale oil has great potential as a resource and has come to be regarded as a strategic successor to conventional resources in oil and gas exploration in China. Recently, a series of important advances have been made in geological research and petroleum exploration in major lacustrine shale strata in the Junggar, Ordos, Songliao, Santanghu, and Bohai Bay basins. These advances have been the result of continuous technological research centered on “sweet spot evaluation, horizontal wells, and volume fracturing” (Kuang et al., 2012, 2014; Zou et al., 2013, 2020; Hu et al., 2018; Zhao et al., 2018; Yang et al., 2019; Jin et al., 2021). Well-controlled resources of the Lucaogou Formation in the Jimsar Sag of the Junggar Basin are more than one billion tons, and the first National Lacustrine Shale Oil Demonstration Area in China has been established in that area. In the Chang 7 Member of the Triassic Yanchang Formation in the Ordos Basin, three shale oil enrichment zones have been confirmed, and several pilot areas (represented by wells X233 and Z183) have been established. A large-scale self-sourced oilfield with one billion tons of reserves has also been discovered in Qingcheng (Yang et al., 2015; Fu et al., 2020). Seven oil-rich zones have been discovered in the Qingshankou Formation in the Songliao Basin, with a total resource scale of more than one billion tons (Guan et al., 2021). Further significant breakthroughs have been made in the Fengcheng Formation in the Mahu Sag of the Junggar Basin, the Jurassic Da'anzhai Member in the Sichuan Basin, and the Permian Lucaogou Formation in the Santanghu Basin (Hu et al., 2019; Wu et al., 2019a; Yang et al., 2019; Jiao et al., 2020; Zhi et al., 2020). In addition, seven oil-rich zones composed of shale

* Corresponding author.
** Corresponding author. Research Institute of Petroleum Exploration and Development, CNPC, Beijing, 100083, China.
E-mail addresses: klc@petrochina.com.cn (L.-C. Kuang), houlh@petrochina.com.cn (L.-H. Hou).

https://doi.org/10.1016/j.petsci.2022.03.005

layers have been identified in the Bohai Bay Basin, including in the Dongying and Zhanhua sags in the Jiyang Depression, the Leijia area and the Damintun sag in the western sag of the Liaohe Depression, the Cangdong and Qikou sags in the Huanghua Depression, and the Shulu sag in the Jizhong depression. Considerable progress has also been made in exploration of the upper Ganchaigou Formation in the Zhahaquan Block, the lower Ganchaigou Formation in the Yingxi Area of the Qaidam Basin, and the first member of the Tengger Formation in the Anan Sag in the Erlian Basin (Zhang et al., 2014; Zhao et al., 2018; Jiao et al., 2020; Jin et al., 2021; Li et al., 2021).

The pore types found in lacustrine shale hydrocarbon reservoirs have obvious differences from the pores in conventional sandstone reservoirs. Lacustrine shale reservoirs are composed of pores that are closely related to both inorganic minerals and organic matter. The development of the pore structures in such reservoirs is profoundly influenced by thermal cracking of organic matter and by inorganic diagenesis, and the evolution of pore-fracture systems is complex. Recently, a number of studies have been conducted on shales using advanced experimental techniques such as FE-SEM, nano-CT, gas adsorption, and high-pressure mercury injection (Zou et al., 2011; Zhu et al., 2013; Wu et al., 2015, 2019a, 2020; Yang and Zou, 2019). These studies have revealed the forming processes and structural complexity of pores in organic-rich lacustrine shales. Two main features are apparent. First, genesis complexity. Both inorganic and organic pores are developed in organic-rich shales. Many interacting factors influence the evolution of porosity, with their relative contributions varying greatly (Wu et al., 2018, 2019a). These factors still need further investigation, in particular, the occurrence state of organic matter in shales and its impact on pores. Second, large differences in pore size. Pore sizes in organic-rich shales vary enormously, ranging from $n \times nm$ to $n \times 10^2 \mu m$. The proportions of pores at different scales also vary greatly between different shales. The sizes and distribution of pores have a considerable influence on shale reservoir performance and oil mobility, although various studies have been conducted, there is as yet no unified understanding of the cause or effect of the variations in these important factors (Chen and Xiao, 2014; Kuang et al., 2014, 2015; Wu et al., 2015, 2019a; Zhu et al., 2016; Zou et al., 2019; Hou et al., 2020a). It is very difficult to quantitatively evaluate organic and inorganic pores in lacustrine shales, and to date, an applicable model has not been established. However, the study of pore structures of lacustrine shales is of great significance as a key factor in “sweet spot area” and “sweet spot section” evaluation in shale oil exploration. It is therefore of vital importance to understand the pore evolution mechanisms of lacustrine shales and to establish suitable pore evaluation models in order to provide scientific guidance and technical support for the large-scale exploration and development of lacustrine shale oil in China.

2. Samples and methods

2.1. Samples

The samples used in this study were primarily organic-matter rich shales from the Upper Triassic Chang 7 member in the Ordos Basin, the Permian Lucaogou Formation in the Junggar Basin, and the Cretaceous Qingshankou Formation in the Songliao Basin. Some organic-matter rich shales from the Silurian Longmaxi Formation in the Sichuan Basin were also used to investigate the effects of maturity on pore volume. Well logging data from Well J174 were collected and were used to verify the new porosity prediction model.

2.2. Methods

TOC content, Rock Eval, X-ray diffraction (XRD), scanning electron microscopy (SEM), helium porosity, and nitrogen adsorption analysis were carried out on the prepared samples to analyze geochemical characteristics, mineralogy, and reservoir quality. Nitrogen adsorption analysis was carried out at Beijing University, and the other experiments were carried out at the National Energy Tight Oil and Gas Research and Development Center, Beijing.

The instruments used for TOC content detection and Rock Eval were a CS-i carbon & sulfur analyzer and a ROCK-EVAL6 pyrolysis apparatus. The experiments were carried out under normal temperature and pressure with samples processed as 200 mesh powders. XRD mineral analysis was conducted on 200 mesh powder samples using a Rigaku SmartLab X-ray diffractometer. An FEI Heilios Nano-lab 650 was used for SEM observation, with a working voltage of 2.00 kV and a working distance of 4.0 mm. Helium porosity was determined using the CoreTest NDP605 AP-608, with the samples being prepared as plungers with diameters of one inch. Kerosene immersion was used to determine the overall volumes of the samples.

Low-pressure nitrogen adsorption experiments were carried out using an ASAP2020 specific surface area analyzer. The samples used were powdered shales with a particle size of 200 mesh. The Brunauer Emmett Teller (BET) model and the Barret Joyner Hallenda (BJH) theory were applied to obtain specific surface areas and pore volumes, respectively. Pores with diameters within the range of 2 nm–200 nm were accessed using nitrogen at 77 K.

3. Distribution of organic matter in shales

There are many types of organic-rich lacustrine shales in China, developed over a long time span and with a wide distribution range. The range of sedimentary environments encompasses ocean, lake, and swamp. To provide sufficient hydrocarbon sources for both conventional and unconventional petroleum accumulations in China, organic-rich shales can be divided into three categories—marine shales, marine-lacustrine transitional shales, and lacustrine shales—according to their original sedimentary environment (Zou et al., 2013, 2019; Jia et al., 2017). Of these types, the maturity of lacustrine organic-rich black shale in petroliferous basins is within the scope of shale oil exploration and development. Shales of this type are found in the Permian petroleum system in the Junggar Basin, the Paleogene petroleum system in the Bohai Bay Basin, the Cretaceous petroleum system in the Songliao Basin, the Triassic petroleum system in the Ordos Basin, and the Jurassic petroleum system in the Sichuan Basin, etc. (Cui et al., 2019; Wu et al., 2019b).

3.1. Distribution patterns of organic matter

The lacustrine basins in China have undergone multiple periods of tectonic transformation, resulting in a short but relatively complex sedimentary evolution process. The types of organic matter found in the lacustrine basins are diverse, frequently with mixed development of sapropelic and humic organic matter. Studies have shown that organic matter types are closely related to structure location and sedimentary facies. Typically, for example, the subsidence centers of large and medium-sized lake basins are generally located in deep lake and semi-deep lake subfacies with shales, rich in sapropelic and partial-sapropelic mixed kerogens. Shallow lakes and delta subfacies are generally the dominant sedimentary types in marginal strata and in the slopes of the basins. Partial-humic

mixed and humic kerogen account for a higher percentage of organic matter in developed shales, with the main bodies of marsh and fluvial shales developing humic kerogen (Zhang et al., 2017; Zou et al., 2019; Li et al., 2021). A study of the organic petrology and SEM analysis of organic-rich shales in different lacustrine basins in China has established that the distribution patterns of organic matter can be divided into three types: laminated continuous distribution, clumped distribution, and stellate scattered distribution.

3.1.1. Laminated continuous distribution

Organic matter with laminated continuous distribution is generally developed in organic-rich shales at semi-deep to deep lacustrine subfacies. Organic matter abundance is high, with TOC generally greater than 3.5% (maximum values exceed 18.87%). Combinations of organic matter and clay-grained minerals are distributed in continuous striated patterns overall, appearing as dark lamellae under a polarized light microscope (Figs. 1-a_1, b_1, c_1) and bright yellow bands under a fluorescence microscope (Figs. 1-b_1, b_2, b_3). These laminae form interbedded layers with slightly coarse-grained felsic and carbonate mineral laminae (Fig. 1). Under FE-SEM, it can be seen that the thickness of a single organic layer is generally less than 10 μm, and that the minerals associated with the organic layer comprise clay minerals (Figs. 1-a_3, c_3) and carbonate minerals (Fig. 1-b_3). Laminated organic matter is an important part of rock structure, bearing overburden pressure. Under the influence of compaction, organic laminae show plastic deformation around rigid particles such as pyrites and apatite (Fig. 1-a_2). In addition, the continuity of the laminae is directly related to the abundance of organic matter. The higher the abundance of organic matter, the greater the continuity and thickness of the organic laminae (Figs. 1-a_3, b_3, c_3).

3.1.2. Clumped distribution

Clumped distribution is the predominant distribution pattern of organic matter in lacustrine shales. Compared to laminated continuous distribution, the principal distinguishing characteristics of clumped distribution are discontinuous and massive accumulations of organic matter, with the particle size of individual lump being relatively large, generally 3–10 times the diameter of shale particles (Fig. 2). Organic matter of this type can be divided into two categories according to internal structure; non-biological structure and biological structure. Based on appearance, organic matter can be further divided into lumpy organic matter and massive organic matter. The first type is represented by long, narrowlumps of organic matter with uniform distribution and uniform internal structure but with no observable components or structure related to the organisms themselves (Fig. 2-a_3). These long, narrow lumps of organic matter usually extend parallel to the direction of bedding, and obvious compression deformation occurs near rigid particles (Fig. 2-a_3). The second type occurs as substantial clumps

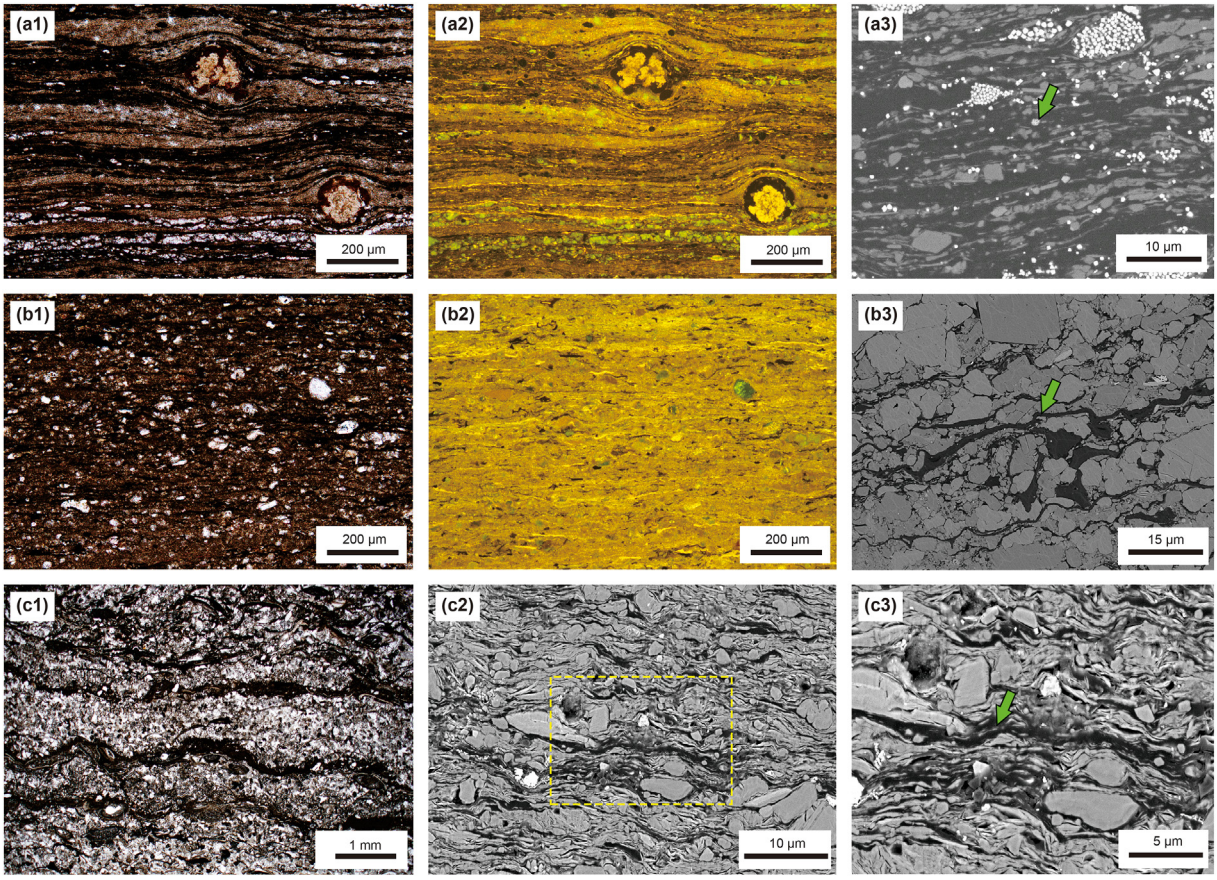

Fig. 1. Characteristics of organic matter in the laminated continuous distribution in lacustrine shales in China.
a_1-a_3 are images of a sample from Well Z70 in the Chang 7_3 sub-member of the Ordos Basin (TOC = 18.87%). a_1 shows the sample under a polarizing microscope, a_2 shows fluorescence under ultraviolet light excitation, and a_3 is an SEM image, with the green arrow indicating organic matter. b_1-b_3 are images of a sample from Well J10022 in the Lucaogou Formation in the Jimsar Sag in the Junggar Basin (TOC = 4.55%). b_1 shows the sample under a polarized light microscope, b_2 shows fluorescence photoexcited by ultraviolet light, and b_3 shows the sample under SEM, with the green arrow indicating organic matter. c_1-c_3 are images of a sample from Well F121 in the Qingshankou Formation in the Songliao Basin (TOC = 3.5%). c_1 shows the sample under a polarized light microscope, c_2 is the sample under SEM, with the area delineated with a broken yellow line indicating the range of image c_3. c_3 is another SEM image, with the green arrow indicating organic matter.

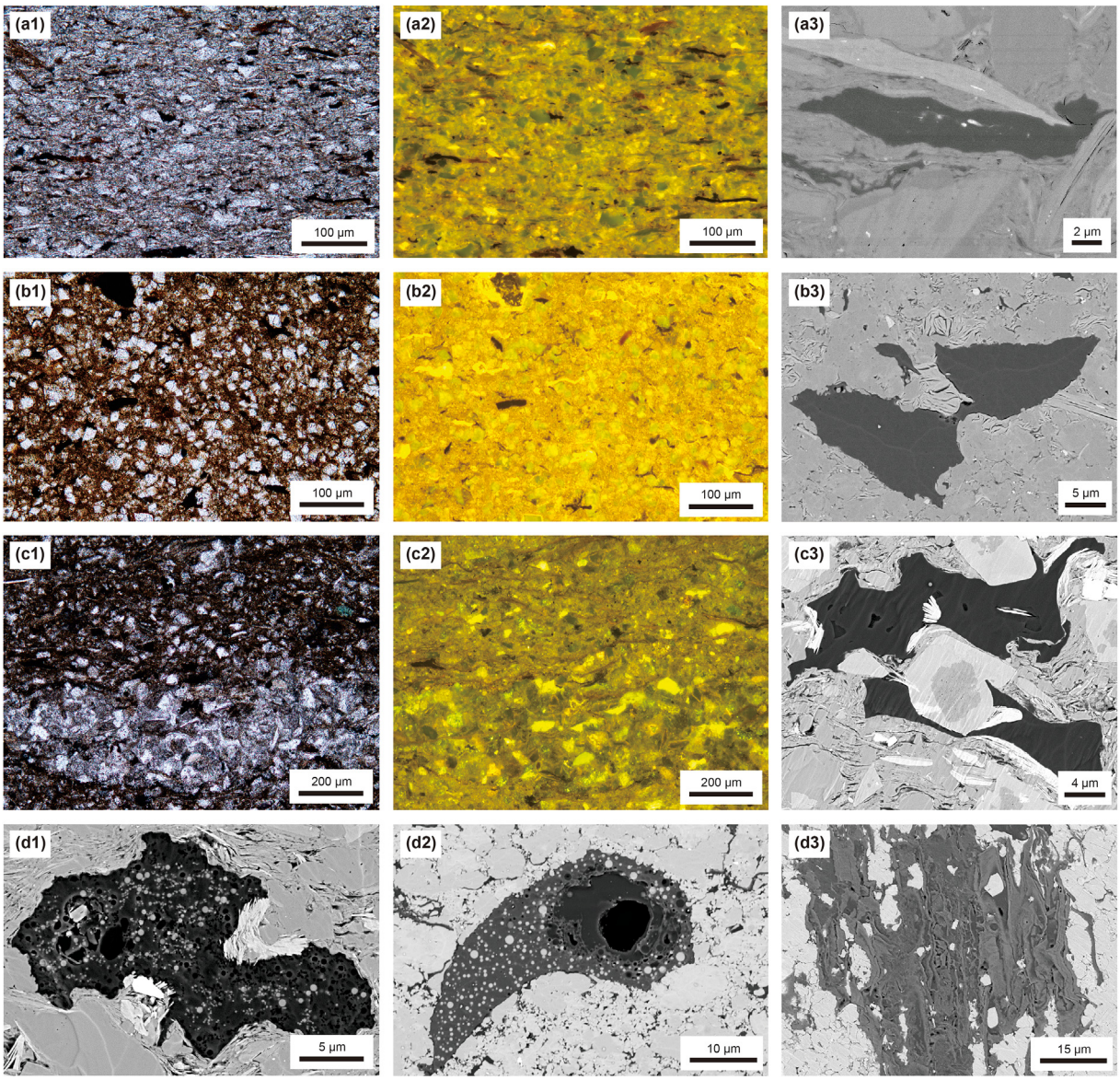

Fig. 2. Characteristics of organic matter with clumped distribution in lacustrine shales in China.
a_1-a_3 are images of a sample from Well L254 in the Chang 7_3 sub-member of the Ordos Basin (TOC = 2.87%). a_1 is the sample under a polarizing microscope, a_2 is under fluorescence with UV excitation, and a_3 is an SEM image. b_1-b_3 are images of a sample from well J10012 in the Lucaogou Formation, in the Jimsar Sag in the Junggar Basin (TOC = 1.85%). b_1 is the sample under a polarized light microscope, b_2 is under fluorescence, excited by ultraviolet light, and b_3 is an SEM image. c_1-c_2 are images of a sample from Well Y16, in the Qingshankou Formation in the Songliao Basin (TOC = 1.5%). c_1 is the sample under a polarized light microscope and c_2 is an image under a fluorescence microscope. c_3 is an SEM image of a sample from Well GY1, in the Qingshankou Formation. d_1 is an SEM image of a sample from Well GY2 in the Qingshankou Formation. d_2 is an SEM image of a sample from Well M705 in the Lucaogou Formation. d_3 is an SEM image of a sample from the Lucaogou Formation in Well J174.

or clusters of organic matter, represented by multiple, interconnected organic matter aggregates (Figs. 2-b_3, c_3). Organic matter of this type has obvious biological structure and the main bodies are distributed in relatively independent blocks with internal spherical apatite (Figs. 2-d_1, d_2) or lattice structures (Fig. 2-d_3). This kind of organic matter is arched, or has sharp edges, and the size of organic matter clusters can reach 30 μm–50 μm. Organic matter generally determines maceral types according to biological structure; for example matrix vitrinite, algae, residual plant tissue filamentous, semi-filamentous, and structural vitrinite macerals. Organic matter distributed in clumps is similar to grains in rock and constitutes a component of the overall skeleton of the rock. Although the organic matter does not form continuous single layers, it has undergone diagenetic evolution and transformation and has a supporting effect within the rock skeleton.

3.1.3. Stellate scattered distribution

Organic matter dispersed in a stellate scattered distribution pattern is generally similar to that found in the clumped distribution, but the organic matter accumulations are smaller. The size of stellate dispersed organic matter accumulations is generally less than 5 μm, which is only one-tenth to one-third of the size of inorganic mineral particles in shales (Fig. 3). This type of organic matter is mainly distributed between dolomite and clay minerals (Figs. 3-a_1, a_2, a_3), between albite and clay minerals (Fig. 3-b_1), within albite grains (Fig. 3-b_2), and between pyrite and quartz grains (Fig. 3-b_3). In terms of the morphology of the organic matter, organic matter in stellate dispersed distribution is generally characterized by small accumulations formed as long, narrow strips, and is often punctate (Fig. 3). Although the volume of stellate dispersed organic matter is smaller than that of clumped

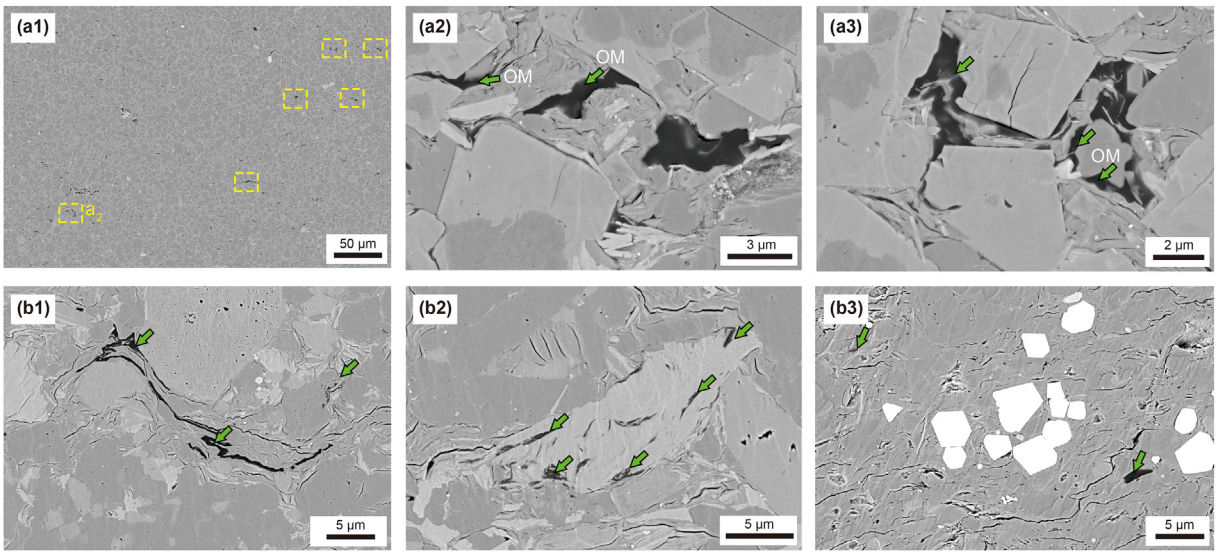

Fig. 3. Characteristics of organic matter with stellate scattered distribution in lacustrine shales in China.
a_1-a_3 are images of a sample from Well J174, in the Lucaogou Formation in the Junggar Basin (TOC = 1.5%). a_1 is a general SEM image of stellate scattered organic matter, a_2 is a local magnification microscope image, a_3 is an SEM image, with the green arrow indicating stellate scattered organic matter. b_1-b_3 are images of a sample from Well Y51, in the Qingshankou Formation in the Gulong area of the Songliao Basin (TOC = 1.29%). b_1 is an SEM image, showing pores between clay minerals filled with narrow banded organic matter. b_2 is an SEM image of the inner pores of albite particles. b_3 is an SEM image showing organic matter distributed in a dispersed band. The green arrows in images b_1-b_3 indicate organic matter.

distributed organic matter, it is also a part of the rock matrix, undergoing diagenetic transformation and bearing overburden pressure. The organic carbon abundance of shales with stellate scattered distribution of organic matter is relatively low, with TOC generally less than 2% (Fig. 3).

In summary, there are obvious differences between the three principal distribution patterns of organic matter found in organic-rich shales. Laminated continuous organic matter is a significant component of rock strata as a whole, and shares the load of overburden pressure with rock clastic particle layers. Organic matter distributed in clumps represents multiple, interconnected particles of rock that constitute components of the overall rock skeleton. Stellate scattered distribution of organic matter generally represents single particles of rock. From laminated continuous distribution of organic matter to clumped distribution of organic matter, and then to stellate scattered distribution of organic matter, the volume of organic matter gradually decreases from large to small, and the distribution pattern gradually changes from continuous to discrete.

4. Shale pore types and pore-forming mechanisms

4.1. Types of shale pores

Compared with conventional sandstone reservoirs, the pores in organic-rich shales are characterized by small pore sizes and poor connectivity (Kenneth et al., 2005; Lu et al., 2015; Zhu et al., 2016; Zou et al., 2019; Wu et al., 2020). For this article, the pore structures of lacustrine shales were studied using field emission SEM. Besides thermal evolution degree, the relationship between pore structure and organic matter occurrence in lacustrine shales was investigated. The results show that the pore structures vary with the different distribution patterns of organic matter.

In shales with laminated continuous distribution of organic matter, the pores consist primarily of intragranular pores of clay minerals such as illite-montmorillonite mixed-layer (Figs. 4-a_1, a_3), albite intragranular pores (Fig. 4-a_2), and pyrite intercrystalline pores (Figs. 4-a_1, a_2). Pore diameters are small, generally ranging between 10 nm and 200 nm. Organic matter pores rarely develop in the interiors and peripheries of lamellar organic matter accumulations.

In shales with clumped distribution of organic matter, the pores are mainly composed of intragranular pores of illite-montmorillonite mixed-layer (Fig. 4-b_1) and dolomite intergranular pores (Fig. 4-b_1). Some intergranular pores are filled with clay minerals (Fig. 4-b_2) because there is a significantly higher proportion of inorganic pores, particularly those related to non-clay minerals. Pore sizes are larger (50 nm–800 nm) compared with shale with continuous laminated organic matter distribution. Although inorganic pores are well developed, organic matter pores are poorly developed, and only a few widely distributed organic matter pores can be observed, as illustrated in Fig. 4-b_3.

In shales with stellate scattered organic matter distribution, dolomite intergranular pores (Fig. 4-c_1) and albite-quartz intergranular pores are the predominant pore types (Figs. 4-c_2, c_3). However, compared with the other two organic matter distribution patterns, organic matter pores are more generally developed. These show three patterns: (1) a slit-like distribution pattern within the organic matter (Fig. 4-c_1); (2) a circular pore-like distribution pattern within the organic matter (Fig. 4-c_2); and (3) slit-like distribution pattern between the organic matter and inorganic minerals (Fig. 4-c_3). In general, the storage spaces of lacustrine shale oil reservoirs in China are dominated by pores related to inorganic minerals, and the proportion of organic pores is relatively low.

4.2. Key controlling factors in shale porosity evolution

Previous major studies have shown that porosity evolution in organic-rich shales is the result of the dual effects of diagenetic evolution of inorganic minerals combined with hydrocarbon generation and expulsion of organic matter (Fishman et al., 2012; Mastalerz et al., 2013; Milliken et al., 2013; Ko et al., 2016; Hou et al., 2020a, 2020b, 2020c, 2021b; Ma et al., 2020a, 2020b). Development of organic pores is more beneficial in improving reservoir performance in shales than inorganic pores (Mayer et al., 2004; Chen and

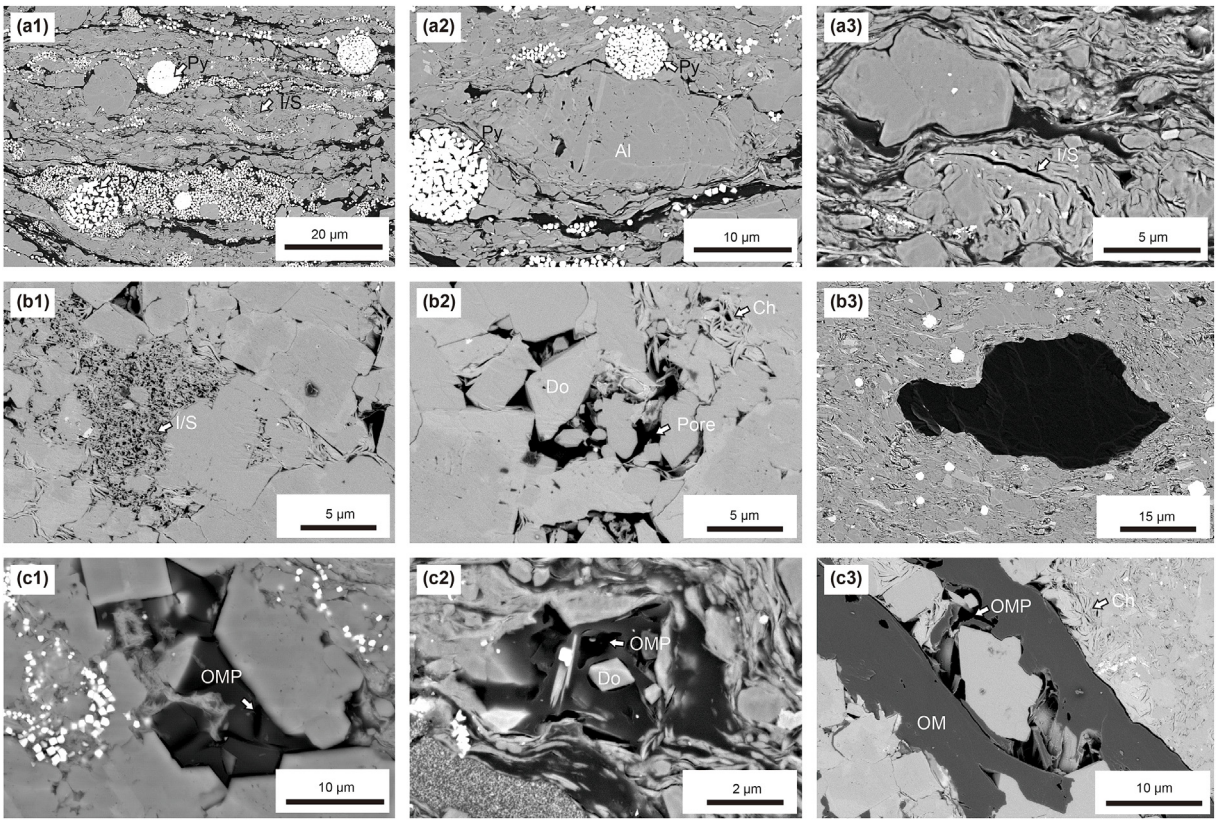

Fig. 4. FE-SEM images of pore structure in lacustrine organic-rich shales.
(a_1) organic matter and clay minerals distributed in a laminar pattern, with inter-pyrite pores and intragranular pores of illite-montmorillonite mixed layers (Chang 7 member, Well Z70). (a_2) intra-albitite pores and intra-pyrite pores (Chang 7 member, Well Z70). (a_3) intragranular pores in illite-montmorillonite mixed layers, with clay minerals and organic matter distributed around quartz and other minerals affected by compaction (Chang 7 member, Well Z70). (b_1) intragranular pores of illite-montmorillonite mixed layers (Lucaogou Formation, Well J174). (b_2) dolomite intergranular pores and chlorite intragranular pores (Lucaogou formation, Well J174). (b_3) organic matter and small intra-matrix pores, with almost no pores visible in the organic matter (Chang 7 member, Well Z70). (c_1) organic matter pores developed inside organic matter, showing straight fracture shapes (Chang 7 member, Well Z70). (c_2) organic pores surrounded by clay minerals such as illite-montmorillonite mixed layer, with dolomite crystals developed within organic matter (Qingshankou Formation, Well F121). (c_3) organic pores and chlorite intragranular pores (Lucaogou Formation, Well J174). Py-Pyrite, OMP-Organic matter pores, Ch-Chlorite, Do-Dolomite, Al-Albite, and I/S-Illite/Smectite mixed layers.

Xiao, 2014; Wu et al., 2015; Zou et al., 2019). The forming of organic pores in shale is affected by various factors such as organic matter type, abundance, maturity, and crude oil cracking degree (Bernard et al., 2012a, 2012b; Mastalerz et al., 2013; Milliken et al., 2013; Bernard and Horsfield, 2014; Cardott et al., 2015; Wu et al., 2019a; Hou et al., 2021).

4.2.1. Organic geochemical parameters

As characteristic components of shale, the types, abundance, and maturity of organic matter have marked effects and controlling influence on the sizes, numbers, and spatial distribution of shale pores, particularly organic pores. Previous studies have shown that, given the same thermal evolution degree, sapropelic organic matter fractions are more likely to develop organic matter pores than humic organic matter fractions (Curtis et al., 2012; Luo et al., 2015; Wu et al., 2019a). This is because pores do not develop easily in humic matter during the thermal evolution of hydrocarbon generation due to the absence of inertinites during the degradation process (Cui et al., 2019). It should be noted that different macerals in kerogen contain different pore types and that the pore types are present in different proportions. For example, vitrinite and algae generally develop micropores and mesopores, while macropores usually develop in residual plant tissues such as the cell cavities of silk bodies, semi-filament bodies, and structural vitrinites (Figs. 2-d_1, d_2). Compared with inertinite and exinite, vitrinite contains a higher proportion of micropores.

Thermal evolution is another important factor affecting the development of organic pores in organic-rich shales (Loucks et al., 2009, 2012; Jarvie et al., 2007; Bernard et al., 2012a). Previous studies have shown that, in the hydrocarbon generation process of shale with the TOC of 7%, consumption of 35% organic carbon could generate a porosity of 4.9%. However, the relationship between thermal evolution maturity and pore development is complex, and the increase in porosity during the process is not linear (Loucks et al., 2009; Curtis et al., 2012; Wu et al., 2019a). Carbonization of organic matter in overmature shales results in reduction of the proportion of organic pores (Zou et al., 2019; Wu et al., 2019a; Wang et al., 2020). Compared with the marine shales of the Longmaxi and Qiongzhusi Formations in the southern Sichuan Basin, the thermal evolution degree of lacustrine shales in China is relatively low, mainly in the range of the oil window. For example, R_o in the Lucaogou Formation generally ranges from 0.7% to 1.1% and R_o in the Chang 7 shale is 0.67%–1.2%. R_o in the Qingshankou Formation is generally slightly higher, ranging between 0.9% and 1.6%. The lower level of thermal maturity is an important reason for limited pore development in lacustrine shale reservoirs compared to marine shales. Fig. 5-a illustrates the relationship between the R_o of different types of shale and the BJH cumulative pore volume. It is found that marine shales have the largest specific pore volume, with a maximum value of 0.043 cm^3/g when R_o is between 2% and 3%. The specific pore volume of lacustrine shale with R_o less than 1.2% (e.g. the Chang 7 member in the Ordos Basin and the Lucaogou

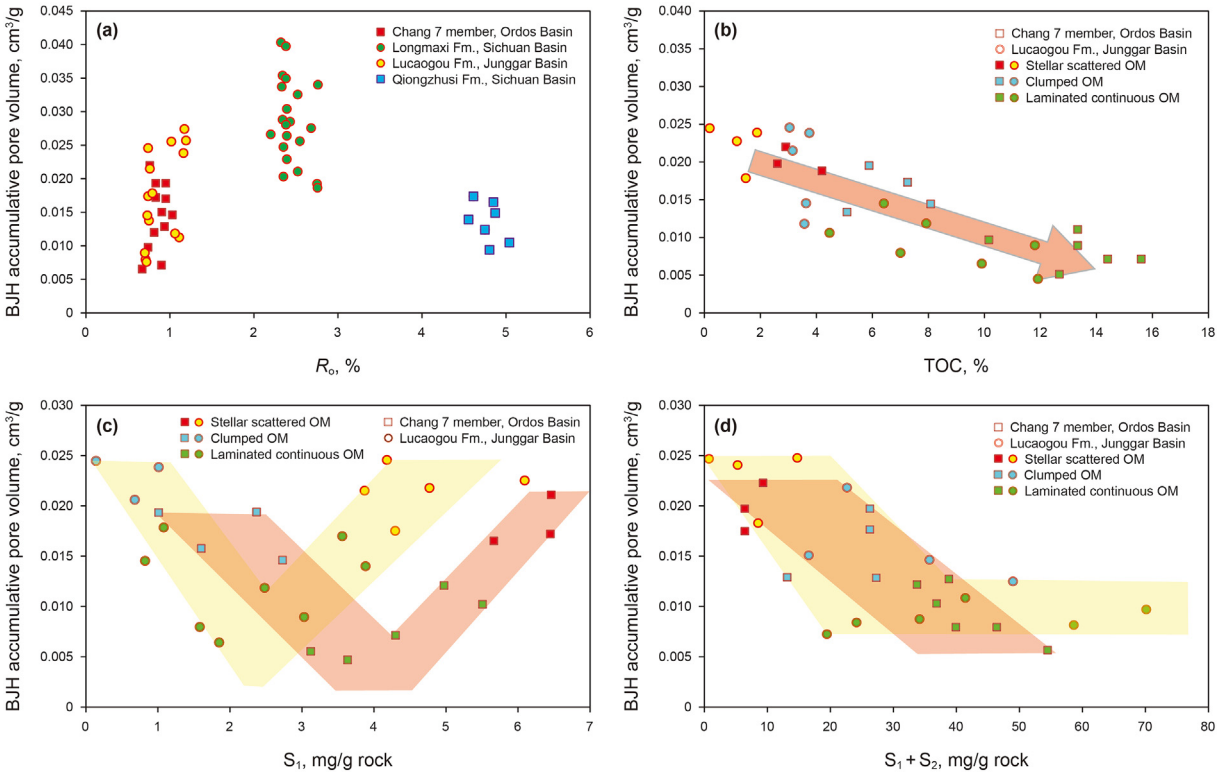

Fig. 5. Scatter diagram of the relationship between BJH accumulative pore volume and organic geochemical parameters.
(a) the relationship between BJH accumulative pore volume and R_o of shales from different regions. (b)–(d): the relationship between BJH accumulative pore volume and the organic geochemical parameters of shales of different organic matter types from the Chang 7 Member in the Ordos Basin and the Lucaogou Formation in the Junggar Basin. (b) is the relationship of BJH accumulative pore volume to TOC; (c) is the relationship of BJH accumulative pore volume to S_1; (d) is the relationship of BJH accumulative pore volume to S_1+S_2.

Formation in the Junggar Basin) is slightly below 0.03 cm^3/g. The pore volume of high-mature shales in the marine Qiongzhusi Formation with $R_o > 4.5\%$ is lower again, with the specific pore volume ranging from 0.01 to 0.02 cm^3/g.

In lacustrine shales with similar maturity, specific pore volumes vary greatly, ranging from 0.005 cm^3/g to 0.03 cm^3/g. The effects of organic matter abundance and pyrolysis S_1 and S_2 on pore volume distribution are further discussed elsewhere in this paper. It can be concluded that, in the Chang 7 Member in the Ordos Basin and the Lucaogou Formation in the Junggar Basin, BJH cumulative pore volume is negatively correlated with TOC. The higher the TOC, the smaller the BJH cumulative pore volume (Fig. 5-b). Pore volume and the pyrolysis peak S_1 show a decreasing trend before increasing. The S_1 peak corresponding to the inflection point in the Chang 7 shale is 4 mg/g rock, and the S_1 peak corresponding to the inflection point in the Lucaogou shale is 2.5 mg/g rock (Fig. 5-c). The BJH cumulative specific pore volume and the hydrocarbon generation potential of S_1+S_2 are generally negatively correlated, showing slightly different trends between the Lucaogou Formation and the Chang 7 Member. The value of S_1+S_2 in the Chang 7 Member decreases incrementally and continuously, while that of the Lucaogou Formation decreases more sharply but then remains stable, with S_1+S_2 corresponding to the inflection point being 20–30 mg/g rock (Fig. 5-d). Analysis of the different distribution forms of organic matter in these shales confirms that the variations in pore volume correspond well with the occurrence of the three types of organic matter distribution. Shales with laminated continuous organic matter distribution have high TOC, low S_1, and high S_1+S_2. Organic matter pores are not developed, and the predominant pore type is clay mineral intragranular pores, resulting in low pore volume (Figs. 4-a-c). The TOC and S_1+S_2 values of shales with clumped distribution of organic matter are medium, but S_1 is low (particularly in the Lucaogou Formation). Although organic matter pores are not developed, the pores are better related to both clay and non-clay minerals, so the pore volume is larger (Figs. 4-d-f). In shales with stellate scattered organic matter distribution, which have a higher proportion of organic filling pores, TOC is relatively low but S_1 is higher, and the content of both organic pores and non-clay mineral pores is higher (Fig. 4-g-i), so the specific pore volume is larger again.

4.2.2. Inorganic mineral composition

Analysis of the pore characteristics of organic-rich shales in different regions and strata both in China and elsewhere has shown that inorganic pores in shale are closely related to clay minerals, plagioclases, and carbonate rocks (Loucks et al., 2009; Wu et al., 2015, 2019b; Zou et al., 2019) and that pore system evolution is affected by the original mineral composition and by diagenetic transformation (Loucks et al., 2009; Cui et al., 2013). In this study, the influence of non-clay and clay minerals on the porosity evolution of both marine and lacustrine shales was analyzed, with shales of the Silurian Longmaxi Formation in the Sichuan Basin, the Triassic Chang 7 member in the Ordos Basin, and the Permian Lucaogou Formation in the Junggar Basin as the research objects. Specific descriptions are as follows:

(1) Non-clay minerals

The relationship with non-clay minerals is the same in both marine and lacustrine shales. BJH cumulative pore volume is positively correlated with quartz content (Fig. 6-a), negatively correlated with plagioclase content (Fig. 6-b), and positively

correlated with dolomite content (Fig. 6-c). During the process of pore evolution, non-clay minerals are affected by organic acids released from organic matter by hydrocarbon generation, resulting in dissolution of existing pores and generation of new pores, of which plagioclase and calcite pores are important types (Loucks et al., 2009; Curtis et al., 2012; Cui et al., 2013; Wu et al., 2015, 2019b; Ko et al., 2016). In lacustrine strata, calcite content is relatively low and plagioclase content is high, indicating a low incidence of dissolution and replacement, so the pore volume is small (Fig. 6-b). Dolomite, an authigenic mineral, forms inside the dissolved pores after calcite dissolution. Higher dolomite content therefore indicates more dissolved pores, so specific pore volume increases (Fig. 6-c). This is consistent with the pore structure of shales in the Lucaogou Formation (Figs. 4-d, e).

(2) Clay minerals

Unlike non-clay minerals, pore volumes of shale reservoirs are generally positively correlated with clay mineral content, but the relationship is more complex (Fig. 6-d). Illite content in the marine shales with R_o greater than 2.0% is high. Illite-montmorillonite mixed layers have transformed into illites and the rock structure tends to be stable. The pore volume of marine shales therefore increases with the growth of illites. However, the pore volumes of lacustrine shales (such as the Lucaogou Formation and the Chang 7 Member) show the opposite trend (Figs. 6-e, f). Pore volumes of marine shales are negatively correlated with the content of illite-montmorillonite mixed-layer, while the pore volumes of lacustrine shales are positively correlated with the content of illite-montmorillonite mixed-layer (Fig. 6-g). Moreover, the correlation between illite content and the pore volume of shale is better than that of illite-montmorillonite mixed layer. This is because, under normal circumstances, illites are distributed in regularly arranged sheets, while illite-montmorillonite mixed layers are haphazardly stacked with wavy montmorillonite and flaked illites. Therefore, when gas adsorption and mercury intrusion detection tests are applied, the pore volume of illites with a more regular arrangement is more readily and accurately obtainable than that of randomly stacked illites in a mixed layer. However, unlike either illites or illite-montmorillonite mixed layer, the correlation between chlorites and the pore volumes of both marine and lacustrine shales is consistent and positive (Fig. 6-h).

4.3. Evolution characteristics of shale pores

The process of pore evolution in organic-rich shales can be divided into four stages. (1) Before hydrocarbon generation: the main pore type in shale is primary inorganic pores and porosity decreases significantly with mechanical compaction (Cui et al., 2013; Lu et al., 2015; Wu et al., 2015, 2016). (2) Oil generation stage: oil generation from organic matter can form nanoscale pores, which are easily filled by oil, and porosity is closely related to residual oil content (Wu et al., 2015; Ko et al., 2016; Wu et al., 2019a). (3) Gas generation stage: nanoscale pores generated in this stage increase shale porosity (Mastalerz et al., 2013; Ko et al., 2016). (4) Over-maturity stage: the hydrocarbon generation potential of organic matter is exhausted and shale porosity will gradually decrease under high temperature and pressure (Ji et al., 2016; Xu et al., 2021; Jiang et al., 2021; Wang, 2020).

For this study, multiple rounds of physical modelling experiments were carried out to investigate the changes in the pores of organic-rich shales during different thermal evolution stages. It was found that shale porosity does not increase linearly, but goes through multiple stages in a five-stage sequence of decreasing, increasing, decreasing again, then increasing continuously and reaching a final relatively stable condition (Fig. 7). The organic-rich lacustrine shales of the Permian Lucaogou Formation in the Junggar Basin are an example. The maturity of the original sample from the Lucaogou Formation was only 0.68%, which represents a low-maturity stage, with few organic pores. When the temperature in the simulation reached 200 °C, R_o reached about 0.7% and the organic matter cracked to produce hydrocarbon, resulting in the appearance of organic matter pores (Wu et al., 2019a). When the temperature in the simulation reached 300 °C, R_o was about 1.0% and the volume and diameter of the pores showed a decreasing trend. When the modelling temperature was about 350 °C, R_o was about 1.2% and organic matter pore volume increased. As the modelling temperature was further increased to 450 °C–550 °C, shale pore volume initially increased and then stabilized (Fig. 7). The decrease in organic matter pores while R_o was in the range of 0.7%–0.9% is probably related to the swelling of organic matter during the hydrocarbon generation process (Wu et al., 2015, 2019a, 2020). From the immature to low-maturity stage, organic matter just begins to crack and generate hydrocarbon so the volume of solid kerogen shrinks, forming long, narrow pores between the organic matter and the mineral matrix, with an overall gradual increase in the occurrence of organic matter pores. After that, in the oil-generation window, the hydrocarbon generation capacity of the organic matter is further enhanced, with the products being mainly liquid hydrocarbons. Undrained liquid hydrocarbons will be adsorbed onto the surface of organic matter, causing swelling and an increase in the volume of organic matter and also resulting in a decrease in the numbers of long, narrow pores between the organic matter and the mineral matrix. In general, the porosity of shales with R_o between 0.7% and 0.9% may therefore be comparatively under-developed.

5. Shale pore evaluation model

5.1. Porosity model

This paper proposes a new model for the evaluation of the organic and inorganic porosity of organic-rich shale based on logging and geological analysis data. It is difficult to distinguish organic and inorganic pores using only logging curves. The model proposed in this paper therefore adopts a combined approach. Total porosity is determined using logging data interpretation. Organic porosity is separately calculated according to established principles. The calculation of inorganic porosity is therefore the difference between total porosity and organic porosity. The basic process for evaluating organic porosity is to first calculate the TOC content of shales using natural gamma spectrometry logging data (Kuang, 1989) and then calculate the organic porosity of shale using the established model of the relationship between TOC content and organic porosity (Christopher and Lapierre, 2012). Kuang (1989) carried out an exhaustive study of natural gamma spectroscopy logging data from shales and confirmed that there is a linear relationship between TOC and the content of the radioactive elements uranium, thorium, and potassium. TOC can therefore be calculated using natural gamma spectrometry logging, as follows (Eq. (1)):

$$\mathrm{TOC} = a \times C_i - b \tag{1}$$

where TOC is the calculated rock organic carbon content (wt.%); a and b are the correlation coefficients (determined according to actual conditions in different areas); and C_i is C_U, C_{Th}, or C_K, representing the contents of uranium, thorium, and potassium in ppm, ppm, and %, respectively.

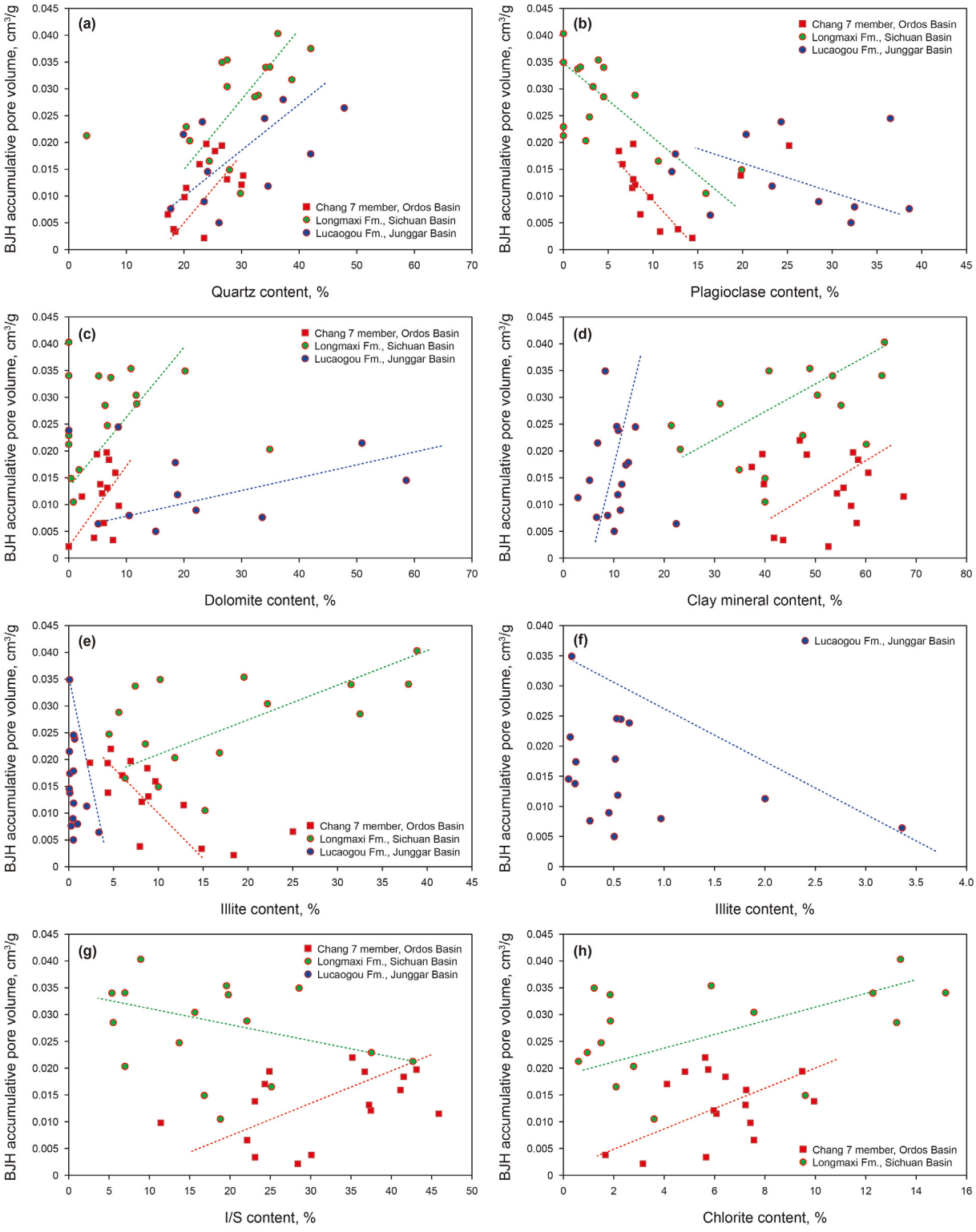

Fig. 6. Scatter diagram of BJH accumulative pore volume and mineral contents.
(a) the relationship between BJH accumulated pore volume and quartz content. (b) the relationship between BJH cumulative pore volume and plagioclase content. (c) the relationship between BJH cumulative pore volume and dolomite content. (d) the relationship between BJH cumulative pore volume and total clay minerals content. (e) the relationship between BJH cumulative pore volume and illite content. (f) the relationship between BJH cumulative pore volume and illite content in the Lucaogou Formation in the Junggar Basin. (g) the relationship between BJH cumulative pore volume and content of illite-montmorillonite mixture layer. (h) the relationship between BJH cumulative pore volume and chlorite content.

The organic matter porosity of the shale can then be estimated by simulation experiment and by the material balance method according to the established principle of shale organic matter pore formation caused by hydrocarbon generation (Christopher et al.,

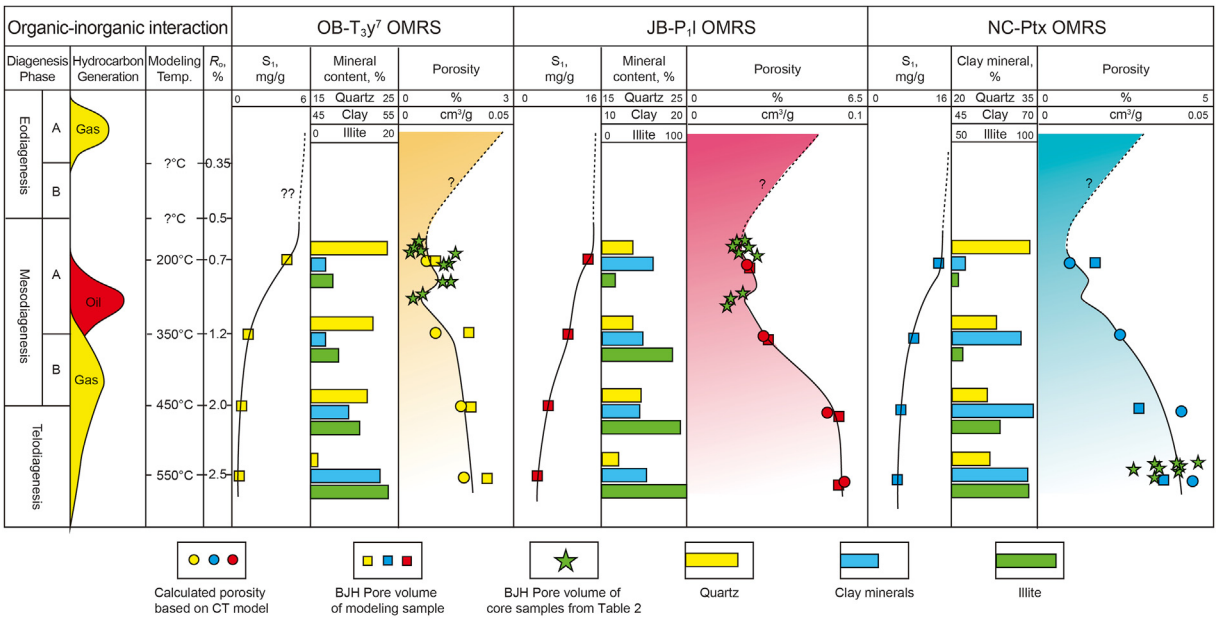

Fig. 7. Pore evolution patterns of different types of shale in China (modified by Wu et al., 2019a).

2012), as follows (Eq. (2)):

$$\Phi_K=(i_{TOC} \times C_c) \times TR \times (\rho_B/\rho_K) \quad (2)$$

where, Φ_K is the porosity of organic matter (%); i_{TOC} is the initial TOC content (wt.%); $i_{TOC} \times C_c$ is the mass of converted organic matter (wt.%); C_c is the dimensionless conversion coefficient related to the original hydrogen index HI_i ($C_c = 0.085 \times HI_i$) (Orr, 1981); TR is the conversion rate associated with maturity ($TR = 100\%/(1 + 20645.5e^{-12.068R_o})$) (%) (Christopher et al., 2013); ρ_B is the rock density, obtained from density logging data (g/cm^3); ρ_K is the kerogen density, evaluated as 1.2 g/cm^3 (Okiongbo et al., 2005; Hou et al., 2021).

In this model, accurate evaluation of total porosity is clearly the key to determining the inorganic porosity of lacustrine shale reservoirs. This is essential for proper evaluation of the effectiveness of shale reservoirs, far more than for conventional reservoirs. There is a fundamental difference between lacustrine shale reservoirs and sandstone reservoirs. Hydrocarbon accumulation in sandstones has the characteristics of "out-sourced migration and enrichment", so that the combination of source and reservoir plays an important role in the evaluation of sandstone reservoirs, and effective porosity is important. Shale oil enrichment, on the other hand, is characterized by a "self-sourced and self-accumulation" model, so it is of crucial importance to obtain a reasonably accurate value for total porosity of the shales in evaluating the effectiveness of shale oil reservoirs.

The matrix density of shale provides a comprehensive reflection of the relative proportions of organic matter and matrix minerals when calculating the total porosity of shale from porosity logging curves. The role of organic matter in different distribution patterns varies significantly. As mentioned, organic matter in a laminated continuous distribution pattern plays a similar role to a 'rock layer', organic matter in a clumped distribution plays a similar role to a part of the 'rock skeleton', and organic matter in a stellate scattered distribution plays a similar role to 'rock particles'. It is therefore necessary to carry out targeted studies in each case, particularly focusing on organic matter that performs a structural role in supporting the rock skeleton, i.e. organic matter in laminated continuous and clumped distributions. The organic porosity is divided accordingly into three different types, and the contributions of the three types OM and their density differences are also considered (Eq. (3)).

$$\Phi_K = \Phi_{K1}+\Phi_{K2}+\Phi_{K3} = a_1(i_{TOC} \times C_c) \times TR \times (\rho_B/\rho_{K1})+ a_2(i_{TOC} \times C_c) \times TR \times (\rho_B/\rho_{K2})+a_3(i_{TOC} \times C_c) \times TR \times (\rho_B/\rho_{K3}) \quad (3)$$

where, Φ_{K1}, Φ_{K2} and Φ_{K3} are organic porosity of OM with laminated continuous distribution, clumped distribution and stellate scattered distribution, respectively, (%). a_1, a_2 and a_3 are percentages of these three types of OM, (wt.%). ρ_{K1}, ρ_{K2}, and ρ_{K3} are kerogen densities of these three types of OM, (g/cm^3).

If the evolution and relative proportions of these types of organic matter are not understood, then a high density of shale mineral skeleton will simply result in a high calculated value for total porosity, which may not accurately reflect actual conditions. In the process of calibrating mineral skeleton density for the accurate measurement of total porosity in the laboratory, it is therefore necessary to consider the occurrence of different types of organic matter so as to obtain a more reasonable value for total porosity.

5.2. Case study

Well J174 in the Permian Lucaogou Formation in the Junggar Basin was selected to carry out porosity evaluation using the new organic matter distribution model. Logging interpretation results show that the total porosity of the Lucaogou Formation is mainly in the range of 7.5%–19.9%, with the porosity of the shale section generally in the range of 2.9%–19.9% (maximum TOC 15.8%) (Fig. 8). The organic porosity of the shale in Well J174 was then calculated according to Eq. (2), using the input parameters shown in Table 1.

The OM under reservoir conditions is ductile and easily deformed if acted upon by additional forces. The heterogeneity of OM-hosted pores can vary significantly among different OM particles (Wang et al., 2020). Different degree of deformation results in different density. The stronger the degree of compaction, the greater the density. The kerogen densities of OM with laminated continuous distribution, clumped distribution, and stellate scattered distribution are 1.3 g/cm^3, 1.2 g/cm^3 and 1.1 g/cm^3,

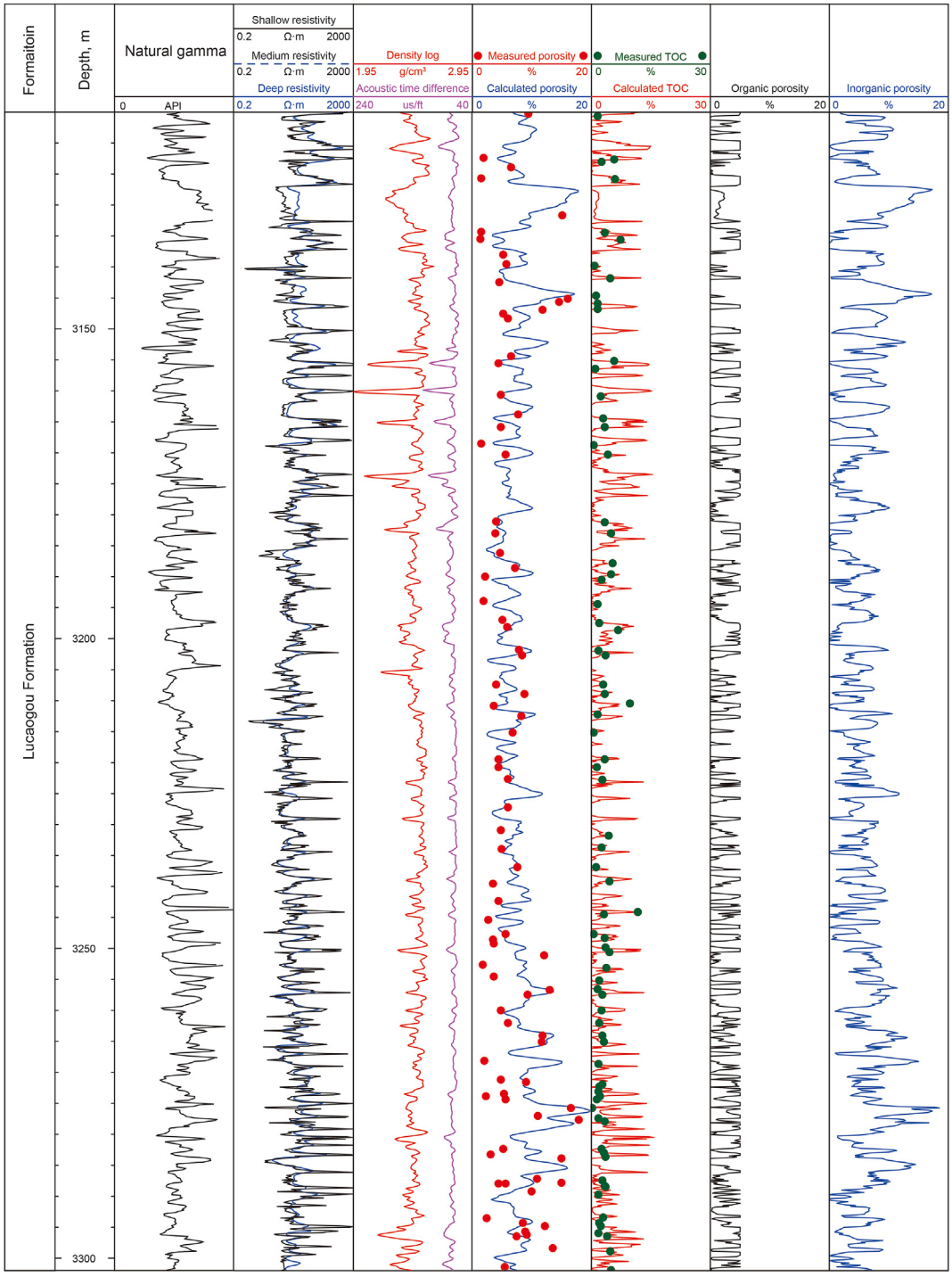

Fig. 8. Porosity evaluation of shales of Lucaogou Formation, Well J174 in the Junggar Basin using logging data.

Table 1
Calculation parameters of shale organic pores in the Junggar Basin.

Basin	Stratum	Porosity, %	Vitrinite reflectance, %	Organic carbon content, %	HI_i, $mg \cdot g^{-1}$	C_c, %	TR, %	ρ_B, g/cm^3	a_1, wt. %	a_2, wt. %	a_3, wt. %	ρ_{K1}, g/cm^3	ρ_{K2}, g/cm^3	ρ_{K3}, g/cm^3
Junggar	Lucaogou Formation	2.9–19.9	0.85	2–15.8	600	51	58	1.95 –2.6	35	40	25	1.3	1.2	1.1

respectively. The most abundant OM is clumped distribution accounting for 40% of TOC, followed by laminated continuous distribution (35 wt. %) and stellate scattered distribution (25 wt. %). The calculation using the new model shows that, under the

influence of hydrocarbon generation, shale porosity increases up to 19.9% but that the large organic pores created cannot be maintained because of strong compaction. According to the chart prepared by Christopher et al. (2012), the maximum organic porosity was accordingly selected as 5% and the calculated organic porosity in Well J174 was corrected based on this value. The overall porosity of organic matter in the Lucaogou Formation was finally calculated to be between 2.5% and 5% and that of inorganic matter between 1% and 6.3%. Porosity calculated using the new model coincides with measured porosity data at a rate of more than 85% (Fig. 8).

6. Conclusion

(1) Based on optical microscope, FE-SEM, and fluorescence microscope observations, the distribution patterns of organic matter in shale can be divided into three types: laminated continuous distribution, clumped distribution, and stellate scattered distribution. Shales with laminated continuous organic matter distribution have high TOC and a relatively low S_1. The TOC of shale with clumped organic matter is medium, and S_1 is low-to-medium. Shales with stellate scattered organic matter have low TOC and relatively high S_1, with a significantly higher proportion of oil filling pores than the other two types.

(2) The pore structures of shale with different distribution patterns of organic matter are different. Shales with laminated continuous distribution and clumped distribution of organic matter are dominated by intra-clay mineral pores and interplagioclase-carbonate pores, with relatively small pore volumes. Organic matter porosity in shales with stellate scattered distribution is comparatively high and pore volumes are large.

(3) Under a certain thermal evolution degree, shale pore volume is negatively correlated with TOC and plagioclase content, but positively correlated with quartz, dolomite, and clay mineral content. Special attention should be paid to illite, chlorite, and illite-montmorillonite mixed layers in clay mineral evaluation. The relationships between different clay minerals and pore volumes are different in different regions.

(4) Multiple rounds of physical modelling experiments and comprehensive evaluation of actual geological conditions in this study showed that the pore evolution of shale undergoes five distinct sequential stages, characterized by porosity decreasing, increasing, decreasing again, and then increasing continually until a final stable condition is reached. Affected by hydrocarbon adsorption and swelling, shales with R_o of 0.8%–1.0% have the lowest porosity.

(5) A new model for the evaluation of organic and inorganic porosity in lacustrine shales is proposed based on well logging interpretation and geological evaluation. The new model was applied in calculating the porosity of shale in the Lucaogou Formation in the Junggar Basin. Total porosity values were derived from logging interpretation. Organic porosity was calculated using the formula set out in the new model. The difference between the two values therefore represented the inorganic porosity. The results of the calculations using the new model indicate that the porosity of organic matter in the Lucaogou Formation shale is 2.5%–5%, and that of inorganic matter is 1%–6.3%. These results coincide with measured data at a rate exceeding 85%.

Acknowledgements

We thank China National Petroleum Corporation's permission to public this paper. This work is sponsored by the National Natural Science Foundation of China (42072187, 42090025), and CNPC Key Project of Science and Technology (2021DQ0405). We thank members of our research community from Xinjiang Oilfield and RIPED for the data and ideas they contributed.

References

Bernard, S., Horsfield, B., Schulz, H.M., et al., 2012a. Geochemical evolution of organic-rich shales with increasing maturity: a STXM and TEM study of the Posidonia Shale (Lower Toarcian, northern Germany). Mar. Petrol. Geol. 31, 70–89. https://doi.org/10.1016/j.marpetgeo.2011.05.010.

Bernard, S., Horsfield, B., 2014. Thermal maturation of gas shale systems. Annual Review of Earth and Planetary 42 (1), 635–651. https://doi.org/10.1146/annurev-earth-060313-054850.

Bernard, S., Wirth, R., Schreiber, A., et al., 2012b. formation of nanoporous pyrobitumen residues during maturation of the barnett shale (fort worth basin). Int. J. Coal Geol. 103, 3–11. https://doi.org/10.1016/j.coal.2012.04.010.

Cardott, B.J., Landis, C.R., Curtis, M.E., 2015. Post-oil solid bitumen network in the Woodford Shale, USA-A potential primary migration pathway. Int. J. Coal Geol. 139 (1), 106–113. https://doi.org/10.1016/j.coal.2014.08.012.

Chen, J., Xiao, X., 2014. Evolution of nanoporosity in organic-rich shales during thermal maturation. Fuel 129 (4), 173–181. https://doi.org/10.1016/j.fuel.2014.03.058.

Christopher, J.M., Lapierre, S.G., 2012. Estimation of kerogen porosity in source rocks as a function of thermal transformation: example from the Mowry Shale in the Powder River Basin of Wyoming. AAPG (Am. Assoc. Pet. Geol.) Bull. 96 (1), 87–108. https://doi.org/10.1306/04111110201.

Cui, J.W., Zhu, R.K., Cui, J.G., 2013. Relationship of porous evolution and residual hydrocarbon: evidence from modeling experiment with geological constrains. Acta Geol. Sin. 87 (5), 730–736.

Cui, J.W., Zhu, R.K., Fan, C.Y., et al., 2019. Oil and gas resources of shale formation orderly accumulation and coexistence as well as its prospecting significance: a case study of Chang 7 shale formation in Ordos Basin. Geol. Bull. China 38 (6), 1052–1061.

Curtis, M.E., Cardott, B.J., Sondergeld, C.H., 2012. Development of organic porosity in the Woodford Shale with increasing thermal maturity. Int. J. Coal Geol. 103 (23), 26–31. https://doi.org/10.1016/j.coal.2012.08.004.

Fishman, N.S., Hackley, P.C., Lowers, H.A., et al., 2012. The nature of porosity in organic-rich mudstones of the upper jurassic kimmeridge clay formation, north sea, offshore United Kingdom. Int. J. Coal Geol. 103, 32–50. https://doi.org/10.1016/j.coal.2012.07.012.

Fu, J.H., Li, S.X., Niu, X.B., et al., 2020. Geological characteristics and exploration of shale oil in Chang 7 member of triassic Yanchang Formation, Ordos Basin, NW China. Petrol. Explor. Dev. 47 (5), 931–945. https://doi.org/10.1016/S1876-3804(20)60107-0.

Guan, M.D., Wu, S.T., Hou, L.H., et al., 2021. Paleoenvironment and chemostratigraphy heterogenity of the Cretaceous organic-rich shales. Advances in Geo-Energy Research 5 (4), 444–455.

Hou, L.H., Luo, X., Han, W.X., et al., 2020c. Geochemical evaluation of the hydrocarbon potential of shale oil and its correlation with different Minerals–a case study of the TYP shale in the Songliao Basin, China. Energy Fuels 34, 11998–12009. https://doi.org/10.1021/acs.energyfuels.0c01285.

Hou, L.H., Luo, X., Zhao, Z.Y., et al., 2021. Identification of oil produced from shale and tight reservoirs in the permian lucaogou shale sequence, jimsar sag, Junggar Basin, NW China. ACS Omega 6 (3), 2127–2142. https://doi.org/10.1021/acsomega.0c05224.

Hou, L.H., Ma, W.J., Luo, X., et al., 2020a. Characteristics and quantitative models for hydrocarbon generation-retention-production of shale under ICP conditions: example from Chang 7 member in the Ordos Basin. Fuel 279, 118497. https://doi.org/10.1016/j.fuel.2020.118497.

Hou, L.H., Ma, W.J., Luo, X., et al., 2020b. Chemical structure changes of lacustrine Type-II kerogen under semi-open pyrolysis as investigated by solid-state 13C NMR and FT-IR spectroscopy. Mar. Petrol. Geol. 116, 104348. https://doi.org/10.1016/j.marpetgeo.2020.104348.

Hou, L.H., Ma, W.J., Luo, X., et al., 2021b. Hydrocarbon generation-retention-expulsion mechanism and shale oil producibility of the permian lucaogou shale in the Junggar Basin as simulated by semi-open pyrolysis experiments. Mar. Petrol. Geol. 125, 104880. https://doi.org/10.1016/j.marpetgeo.2020.104880.

Hu, S.Y., Zhu, R.K., Wu, S.T., et al., 2018. Profitable exploration and development of continental tight oil in China. Petrol. Explor. Dev. 45 (4), 737–748. https://doi.org/10.11698/PED.2018.04.20 (In Chinese).

Hu, Y.J., Wang, Y.S., Huang, S.Q., et al., 2019. The Geological Conditions, Resource Potential,and Exploration Direction of Oil in Liaohe Depression, vol. 24, pp. 43–54, 2.

Jarvie, D.M., Hill, R.J., Tim, T.E., et al., 2007. Unconventional shale gas systems:The Mississippian Barnett shale of North Central Texas as one model for thermogenic shale gas assessment. AAPG (Am. Assoc. Pet. Geol.) Bull. 91 (4), 475–499. https://doi.org/10.1306/12190606068.

Ji, L.M., Wu, Y.D., He, C., et al., 2016. High pressure simulation of organic-rich mudstone and shale for hydrocarbon generation and pore evolution. Acta Geol. Sin. 37 (2), 172–181. https://doi.org/10.7623/syxb201602003.

Jia, C.Z., Zheng, M., Zhang, J.F., 2017. Breakthrough and significance of unconventional oil and gas to classical petroleum geological theory. Petrol. Explor. Dev.

44 (1), 1–11. https://doi.org/10.11698/PED.2017.01.01.
Jiang, X.H., Wu, S.T., Hou, L.H., 2021. Porosity evolution In lacustrine organic-matter-rich shales with high claly minerals content. Frontiers in Earth Science 9, 7660936. https://doi.org/10.3389/feart.2021.766093.
Jiao, F.Z., Zou, C.N., Yang, Z., 2020. Geological theory and exploration & development practice of hydrocarbon accumulation inside continental source kitchens. Petrol. Explor. Dev. 47 (6), 1147–1159. https://doi.org/10.1016/S1876-3804(20)60125-8.
Jin, Z.J., Bai, Z.R., Gao, B., et al., 2021. Has China ushered in the shale oil and gas revolution? Petroleum Knowledge (2), 24–25. https://doi.org/10.11743/ogg20190301.
Kenneth, S.O., Aplin, A.C., Larter, S.R., 2005. Changes in type II kerogen density as a function of maturity: evidence from the kimmeridge clay formation. Energy Fuels 19, 2495–2499. https://doi.org/10.1021/ef050194.
Ko, L.T., Loucks, R.G., Zhang, T.W., et al., 2016. Pore and pore network evolution of Upper Cretaceous Boquillas (Eagle Ford–equivalent) mudrocks: results from gold tube pyrolysis experiments. AAPG (Am. Assoc. Pet. Geol.) Bull. 100 (11), 1693–1722. https://doi.org/10.1306/04151615092.
Kuang, L.C., 1989. Using natural gamma spectrometry logging data to evaluate the organic matter abundance of claystone. Well Logging Technol. (6), 39–42+75.
Kuang, L.C., Tang, Y., Lei, D.W., et al., 2012. Formation conditions and exploration potential of tight oil in the Permian saline lacustrine dolomitic rock, Junggar Basin, NW China. Petrol. Explor. Dev. 39 (6), 657–667.
Kuang, L.C., Gao, G., Xiang, B.L., et al., 2014. Lowest limit of organic carbon content in effective source rocks from Lucaogou Formation in Jimusar Sag. Petrol. Explor. Dev. 36 (2), 224–229. https://doi.org/10.11781/sysydz201402224.
Kuang, L.C., Wang, X.T., Guo, X.G., et al., 2015. Geological characteristics and exploration practice of tight oil of Lucaogou formation in jimsar sag. Xinjing Pet. Geol. 36 (6), 629–635. https://doi.org/10.7657/XJPG20150601.
Loucks, R.G., Reed, R.M., Ruppel, S.C., et al., 2012. Spectrum of pore types and networks in mudrocks and a descriptive classification for matrix-related mudrock pores. AAPG (Am. Assoc. Pet. Geol.) Bull. 96 (6), 1071–1098. https://doi.org/10.1306/08171111061.
Li, M.Y., Wu, S.T., Hu, S.Y., et al., 2021. Lamination Texture and Its Effects on Reservoir and Geochemical Properties of the Palaeogene Kongdian Formation in the Cangdong Sag, Bohai Bay Basin, China. Minerals 11 (12), 1360. https://doi.org/10.3390/min11121360.
Loucks, R.G., Reed, R.M., Ruppel, S.C., 2009. Morphology, genesis, and distribution of nanometer-scale pores in siliceous mudstones of the Mississippian Barnett Shale. J. Sediment. Res. 79 (12), 848–861. https://doi.org/10.2110/jsr.2009.092.
Lu, J., Ruppel, S.C., Rowe, H.D., 2015. Organic matter pores and oil generation in the Tuscaloosa marine shale. AAPG (Am. Assoc. Pet. Geol.) Bull. 99 (2), 333–357. https://doi.org/10.1306/08201414055.
Luo, X.R., Wu, P., Zhao, J.H., et al., 2015. Study Advances on Organic Pores in Organic Matter-Rich Mud Shale, vol. 42, pp. 50–59, 1.
Ma, W., Hou, L., Luo, X., et al., 2020a. Role of bitumen and NSOs during the decomposition process of a lacustrine Type-II kerogen in semi-open pyrolysis system. Fuel 259, 116211. https://doi.org/10.1016/j.fuel.2019.116211.
Ma, W., Hou, L., Luo, X., et al., 2020b. Generation and expulsion process of the Chang 7 oil shale in the Ordos Basin based on temperature-based semi-open pyrolysis: implications for in-situ conversion process. J. Petrol. Sci. Eng. 186, 106710. https://doi.org/10.1016/j.petrol.2020.107035.
Mastalerz, M., Schimmelmann, A.D.A., Chen, Y., 2013. Porosity of Devonian and Mississippian new Albany shale across a maturation gradient: insights from organic petrology, gas adsorption and mercury intrusion. AAPG (Am. Assoc. Pet. Geol.) Bull. 97, 1621–1643. https://doi.org/10.1306/04011312194.
Mayer, L.M., Schick, L.L., Hardy, K.R., et al., 2004. Organic matter in small mesopores in sediments and soils. Geochem. Cosmochim. Acta 68 (19), 3863–3872. https://doi.org/10.1016/j.gca.2004.03.019.
Milliken, K.L., Rudnicki, M., Awwiller, N.D., 2013. Organic matter-hosted pore system, marcellus formation (devonian), Pennsylvania. AAPG (Am. Assoc. Pet. Geol.) Bull. 97 (2), 177–200. https://doi.org/10.1306/07231212048.
Okiongbo, K.S., Aplin, A.C., Larter, S.R., 2005. Changes in type II kerogen density as a function of maturity: evidence from the kimmeridge clay formation. Energy Fuels 19, 2495–2499. https://doi.org/10.1021/ef050194.
Wang, G.C., 2020. Deformation of organic matter and its effect on pores in mud rocks. AAPG (Am. Assoc. Pet. Geol.) Bull. 103 (1), 21–36. https://doi.org/10.1306/04241918098.
Wang, Y.M., Li, J., Wang, H., et al., 2020. Prediction of organic matter carbonization zones for lower silurian Longmaxi Formation in middle-upper yangtze region. Natural Gas Geoscience 31 (2), 151–162. https://doi.org/10.11764/j.issn.1672-1926.2019.12.009.
Wu, S.T., Yang, Z., Zhai, X.F., et al., 2019a. An experimental study of organic matter, minerals and porosity evolution in shales within high-temperature and high-pressure constraints. Mar. Petrol. Geol. 102, 377–390. https://doi.org/10.1016/j.marpetgeo.2018.12.014.
Wu, S.T., Zhu, R.K., Yang, Z., et al., 2019b. Distribution and characteristics of lacustrine tight oil reservoirs in China. J. Asian Earth Sci. 178, 20–36. https://doi.org/10.1016/j.jseaes.2018.05.013.
Wu, S.T., Zou, C.N., Zhu, R.K., et al., 2015. Reservior quality characterization of upper triassic Chang 7 shale in Ordos Basin. Earth Sci. J. China Univ. Geosci. 40 (11), 1810–1823 (in Chinese).
Wu, S.T., Zhu, R.K., Cui, J.W., et al., 2020. Ideas and prospect of porous structure characterization in unconventional reservoirs. Geol. Rev. 66, 151–154 (in Chinese).
Wu, S.T., Zhu, R.K., Li, X., et al., 2018. Evaluation and application of porous structure characterization technologies in unconvertional tight reservoirs. Earth Sci. Front. 25 (2), 191–203 (in Chinese).
Xu, J.L., Wu, S.T., Liu, J.D., 2021. New insights into controlling factors of pore evolution in organic-rich shale. Energy & Fuels 35, 4858–4873. https://doi.org/10.1021/acs.energyfuels.0c04189.
Yang, H., Niu, X.B., Xu, L.M., et al., 2015. Reservoir quality characterization of upper triassic Chang 7 shale in Ordos Basin. Earth Sci. J. China Univ. Geosci. 43 (4), 511–520 (in Chinese).
Yang, Y.M., Huang, D., Yang, G., et al., 2019. Geological conditions to form lacustrine facies shale oil and gas of Jurassic Daanzhai Member in Sichuan Basin and exploration directions. Nat. Gas Explor. Dev. 42 (2), 1–12 (in Chinese).
Yang, Z., Zou, C.N., 2019. Exploring petroleum inside source kitchen": connotation and prospects of source rock oil and gas. Petrol. Explor. Dev. 46 (1), 173–184. https://doi.org/10.11698/PED.2019.01.18.
Zhang, L.Y., Bao, Y.S., Li, J.Y., et al., 2014. Movability of lacustrine shale oil:A case study of dongying sag, Jiyang depression, Bohai Bay Basin. Petrol. Explor. Dev. 41 (6), 641–649. https://doi.org/10.11698/PED.2014.06.01.
Zhang, S.C., Liang, D.G., Chen, J.P., et al., 2017. Origin and Distribution of Marine Petroleum Accumulation in China. Science Press, Beijing, pp. 1–150 (in Chinese).
Zhao, W.Z., Hu, S.Y., Hou, L.H., 2018. Connotation and strategic role of in-situ conversion processing of shale oil underground in the onshore China. Petrol. Explor. Dev. 45 (4), 537–545. https://doi.org/10.11698/PED.2018.04.01.
Zhao, X.Z., Zhou, L.H., Pu, X.G., et al., 2018. Geological characteristics of shale rock system and shale oil exploration breakthrough in a lacustrine basin: a case study from the Paleogene 1st sub-member of Kong 2 Member in Cangdong sag, Bohai Bay Basin, China. Petrol. Explor. Dev. 45 (3), 361–372. https://doi.org/10.11698/PED.2018.03.01.
Zhi, D.M., Tang, Y., He, W.J., et al., 2020. Orderly coexistence and accumulation models of conventional and unconventional hydrocarbons in lower permian Fengcheng Formation, Mahu sag, Junggar Basin. Petrol. Explor. Dev. 48 (1), 38–51. https://doi.org/10.11698/PED.2021.01.04 (In Chinese).
Zhu, R.K., Bai, B., Cui, J.W., et al., 2013. Research advances of microstructure in unconventional tight oil and gas reservoirs. J. Palaeogeogr. 15 (5), 615–623. https://doi.org/10.7605/gdlxb.2013.05.049.
Zhu, R.K., Wu, S.T., Su, L., et al., 2016. Problems and future works of porous texture characterization of tight reservoirs in China. Acta Pet. Sin. 37 (11), 1323–1336. https://doi.org/10.7623/syxb201611001 (in Chinese).
Zou, C.N., Zhu, R.K., Bai, B., et al., 2011. First discovery of nano-pore throat in oil and gas reservoir in China and its scientific value. Acta Petrol. Sin. 27 (6), 1857–1864 (in Chinese).
Zou, C.N., Yang, Z., Cui, J.W., et al., 2013. Formation mechanism, geological characteristics and development strategy of nonmarine shale oil in China. Petrol. Explor. Dev. 40 (1), 14–26.
Zou, C.N., Pan, S.Q., Jing, Z.H., et al., 2020. Shale oil and gas revolution ang its impact. Acta Pet. Sin. 41 (1), 1–12.
Zou, C.N., Zhu, R.K., Chen, Z.Q., et al., 2019. Organic-matter-rich shales of China. Earth Sci. Rev. 189, 51–78. https://doi.org/10.1016/j.earscirev.2018.12.002.